CONF-9209143

Backlash Control via Redundant Drives: An Experimental Verification

Lung-Wen Tsai
Professor
Fellow ASME

Sun-Lai Chang*
Graduate Research Assistant

Mechanical Engineering Department
and
Systems Research Center
The University of Maryland
College Park, MD 20742

CONF-9209143--1

DE92 016368

ABSTRACT

In this paper, a novel concept for the control of backlash in geared servo-mechanisms is demonstrated with a prototype manipulator. The concept utilizes unidirectional redundant drives to assure positive coupling of gear meshes at all times and, thereby, eliminates backlash completely. To establish a proof of concept, a two-DOF prototype manipulator with three unidirectional drives is designed and tested. Dynamic model based on Lagrange's formulation is established. A PID controller using computed torque control technique is developed. Two experiments, one with redundant drives and the other without redundant drives, are conducted. The experimental results demonstrate that use of unidirectional redundant drives improves the repeatability of a manipulator by an order of magnitude.

INTRODUCTION

Most mechanical systems and servomechanisms employ gear trains for power transmission and torque amplification. Backlash is a persistent problem in such machines due to natural clearances provided for prevention of jamming of gear teeth due to manufacturing errors and/or thermal expansion. Gear backlash introduces discontinuity and impact in mechanical systems which, in turn, make control of a machine difficult. The positioning accuracy of a servomechanism is also compromised due to backlash.

Various methods such as antibacklash gears (Michalec, 1966), adjustable tooth thickness gears (Michalec, 1966), adjustable center distance (Dagalakis and Myers, 1985), and harmonic drives (Calson, 1985) have been proposed for elimination of gear backlash. Using these methods, some improvement on problems caused by backlash has been made. However, these techniques do not completely eliminate backlash and can further increase the cost of manufacturing and assembling such machines.

*Currently with the United Parcel Service, Research and Development, Danbury, CT 06810.

In the past decade, advances in microelectronics and power electronics have transformed analog servo systems into highly reliable all digital systems. These modern servo systems are usually implemented with digital signal processing chips. All the loop are closed with digital algorithms which make it possible to implement a broad range of control algorithms based on recent advances in digital control theory. Special functions can be built into these digital control algorithms to compensate for backlash and to improve the accuracy of a machine (Veitschegger and Wu, 1986, Sweet, 1991). This seems to be a promising approach. However, it still can not eliminate backlash positively and completely.

In a previous paper, we introduced a new and innovative concept for the control of backlash (Chang and Tsai, 1990b). The concept utilizes unidirectional redundant drives to assure positive coupling of gear meshes at all times and, thereby, eliminates backlash completely. In this paper, we demonstrate the concept via a two-DOF (Degree-Of-Freedom) prototype manipulator. First, the general principle of operation for RBR (Redundant-drive Backlash-free Robotic) mechanisms will be briefly reviewed. Then the kinematics, dynamics, and control of the prototype manipulator will be derived. Redundant motor torques based on minimum power consumption will be resolved. Power consumption for such a RBR servomechanism with and without redundant drives will be derived and compared. Finally, experimental results confirming the improvement in repeatability will be presented.

PRINCIPLE OF OPERATION

Chang and Tsai (1990b) introduced the concept of RBR mechanisms and showed that a minimum of $(n+1)$ properly arranged unidirectional drives are needed for the control of backlash in an n-DOF manipulator. For an n-DOF mechanism with $(n+1)$ unidirectional drives, they showed that the input angular displacements and joint angles are related by the following

This paper has been accepted for presentation at the 22nd ASME Biennial Mechanisms Conference, Scottsdale, Az., Sept. 1992.

FG05-88ER13977

linear transformation

$$\phi = B\,\theta, \tag{1}$$

where $\theta = [\theta_1, \theta_2, \cdots, \theta_n]^T$ is the joint angles, $\phi = [\phi_1, \phi_2, \cdots, \phi_{n+1}]^T$ is the actuator displacements, and $B = [b_{ij}]$ is an $(n+1) \times n$ matrix. Note that the word *"joint"* refers to the joint in the *equivalent open loop chain* of a geared robotic mechanism defined by Tsai (1988).

They also showed that the resultant joint torques are related to input actuator torques by:

$$\underline{\tau} = A\,\underline{\xi}, \tag{2}$$

where $\underline{\tau} = [\tau_1, \tau_2, \cdots, \tau_n]^T$ denotes the resultant joint torques, $\underline{\xi} = [\xi_1, \xi_2, \cdots, \xi_{n+1}]^T$ the input actuator torques, and $A = B^T$ the *structure matrix* (Chang and Tsai, 1990a).

The structure matrix is a function of mechanism structural topology and gear ratios. The $i-th$ row describes how the resultant torque about the $i-th$ joint axis is affected by the input actuators, while the $j-th$ column describes how the $j-th$ actuator torque is transmitted to various joints. For this reason, each column vector in the structure matrix and its corresponding gear train is called a *transmission line*. The structure matrix for an n-DOF mechanism with $n+1$ unidirectional drives obeys the following rules.

R1. The transmission lines form an $n \times (n+1)$ structure matrix and each row must contain at least two non-zero elements.

R2. The sub-matrix obtained by deleting any column from the structure matrix is non-singular.

R3. Since actuator torques are transmitted to various joints via gear trains, non-zero elements in a column of the structure matrix must be consecutive.

R4. Switching any two columns of a structure matrix results in a renumbering of the two corresponding input actuators. Two kinematic structures are said to be isomorphic if their structure matrices become identical after one or repeated operations of column exchanges.

Rules 1 and 2 ensure the unidirectional controllability of a mechanism. A special characteristic for this type of mechanisms is that, given a set of desired joint torques, the solution for actuator torques is an indeterminate problem. Specifically, Eq. (2) consists of n linear equations in $n+1$ unknowns. Hence, the solution for the required actuator torques can be written as (Klein and Huang, 1983):

$$\underline{\xi} = A^{+}\underline{\tau} + \lambda\,\underline{\mu} \tag{3}$$

$$\begin{bmatrix} \# & \# & \# \\ \# & \# & \# \end{bmatrix} \quad \begin{bmatrix} \# & \# & \# \\ \# & \# & 0 \end{bmatrix} \quad \begin{bmatrix} \# & \# & 0 \\ \# & \# & \# \end{bmatrix} \quad \begin{bmatrix} \# & \# & 0 \\ \# & 0 & \# \end{bmatrix}$$

$g^3 - 1$ $\quad$ $g^3 - 2$ $\quad$ $g^2s - 1$ $\quad$ $g^2s - 2$

Table 1: Admissible 2-DOF Structure Matrices

where $\underline{\mu} = [\mu_1, \mu_2, \cdots, \mu_{n+1}]^T$ denotes the null vector of A, $A^{+} = A^T(A\,A^T)^{-1}$ denotes the pseudo inverse of A, and λ is an arbitrary real number.

The first term on the right hand side of Eq. (3) is called the *particular solution* and the second term, which results in no net joint torques, is called the *homogeneous solution*. Hence, regardless of the value of $\underline{\tau}$, the sense of input torques, $\underline{\xi}$, can be kept in the same direction of the null vector, $\underline{\mu}$, by selecting a proper positive value of λ. Similarly, it can also be kept in the opposite direction of the null vector by selecting a proper negative value of λ. Since each actuator torque can be maintained in a predetermined direction at all times, gear backlash will never occur.

PROTOTYPE RBR ARM

To establish a proof of the concept, a two-DOF prototype arm with three unidirectional drives is designed. There are four admissible structure matrices for two-DOF RBR mechanisms as shown in Table 1, where a "# " sign denotes the existence of a non-zero element. The last structure matrix listed in Table 1 is selected for the design because of its simplicity in coupling.

Figure 1 shows the schematic diagram of the arm. To simplify the formulation of dynamical equations, two or more components keyed together with a common shaft are considered as one rigid link. In the prototype design, both joint axes are parallel to the direction of gravity to reduce the gravitational effect and the link lengths are equal to one another to maximize the workspace. There are three transmission lines driven by three motors as shown in Fig. 1. The first two motors (actuators) are connected to the ground and the third is installed on the rear-end of the first moving link. Motor 1 drives both joints 1 and 2 simultaneously, while motor 2 drives joint 1 and motor 3 drives joint 2, independently. A two-stage gear reduction is used between each motor and the first joint it drives. Motors 1 and 2 are Electro-Craft 0588-33-501 DC motors and motor 3 is a Pittman 14203 DC motor.

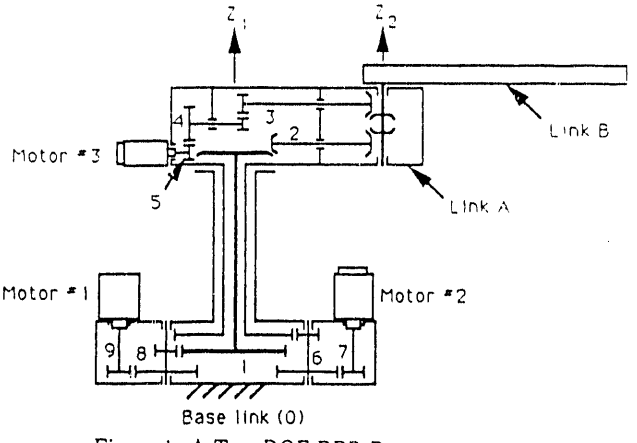

Figure 1: A Two-DOF RBR Prototype Arm.

Two sensors are sufficient for feedback control of the manipulator. Since motors 2 and 3 drive joints 1 and 2, respectively, one sensor is placed on each shaft of the two motors for sensing the joint angles and joint angular velocities of the robot arm.

The gear ratios used in the design are as follows: $N_{8,9} = N_{1,8} = N_{6,7} = N_{1,6} = 96/15, N_{4,5} = 120/24, N_{3,1} =$

$N_{8,9} = 20/40$, $N_{2,A} = 16/64$, $N_{B,2} = 12/24$, and $N_{B,3} = 20/40$, where $N_{i,j} = N_i/N_j$ denotes the ratio of the numbers of teeth on the gear pair attached to links i and j.

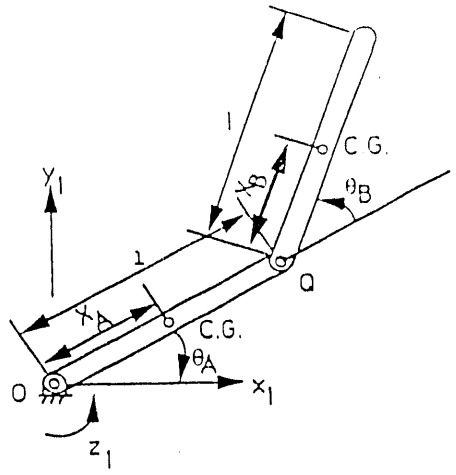

Figure 2: Equivalent open-loop chain of the mechanism shown in Fig.1.

KINEMATIC EQUATIONS

Figure 2 shows the equivalent open-loop chain for the manipulator shown in Fig. 1. All links contained in the equivalent open-loop chain are called the *major links* or the *carriers*, and those not contained in the equivalent open-loop chain are called the *carried links*. As shown in Fig. 2, links A and B are two moving carriers and link 0 is a fixed carrier. Link 0 carries links 1, 6, 7, 8, and 9; link A carries links 2, 3, 4 and 5; while link B does not carry any link.

Relative motions of the carried links with respect to their corresponding carriers can be derived by the theory of *fundamental circuits* and the *coaxiality condition* (Tsai, 1988). For example, link A serves as the carrier for the gear pair attached to links 2 and B shown in Fig. 1. Hence, the pair of gears attached to links 2 and B, and link A form a fundamental circuit. The fundamental circuit equation can be written as:

$$\dot{\theta}_{2,A} = N_{B,2}\dot{\theta}_{B,A} \tag{4}$$

where $\theta_{i,j}$ denotes the relative rotation of link i with respect to link j, and the "dot" denotes its time derivative.

Similarly, link A also serves as the carrier for the gear pair attached to links 1, 2. The fundamental circuit equation is:

$$\dot{\theta}_{1,A} = N_{2,1}\dot{\theta}_{2,A} \tag{5}$$

It can be seen from Fig. 1 that links 0, 1, and A share a common joint axis, Z_1. The coaxiality condition among these three links can be written as:

$$\dot{\theta}_{1,A} = \dot{\theta}_{1,0} - \dot{\theta}_{A,0} \tag{6}$$

Substituting Eqs. (4) and (6) into (5) and after simplification, yields

$$\dot{\theta}_{1,0} = \dot{\theta}_{A,0} + N_{2,1}N_{B,2}\dot{\theta}_{B,A} \tag{7}$$

Equations (4) and (7) express angular velocities of links 2 and 1, with respect to their carriers, in terms of the joint angular velocities. Similarly, angular velocities of links 3 to 9 can be derived. After substituting numerical values of the gear ratios, the resulting equations are:

$$\dot{\theta}_{1,0} = \dot{\theta}_A + 0.125\dot{\theta}_B \tag{8}$$

$$\dot{\theta}_{2,A} = 0.5\,\dot{\theta}_B \tag{9}$$

$$\dot{\theta}_{3,A} = -2.0\dot{\theta}_B \tag{10}$$

$$\dot{\theta}_{4,A} = 4.8\dot{\theta}_B \tag{11}$$

$$\dot{\theta}_{5,A} = -24\dot{\theta}_B \tag{12}$$

$$\dot{\theta}_{6,0} = -6.4\dot{\theta}_A \tag{13}$$

$$\dot{\theta}_{7,0} = 40.96\dot{\theta}_A \tag{14}$$

$$\dot{\theta}_{8,0} = -6.4\dot{\theta}_A - 0.8\dot{\theta}_B \tag{15}$$

$$\dot{\theta}_{9,0} = 40.96\dot{\theta}_A + 5.12\dot{\theta}_B \tag{16}$$

where $\theta_A = \theta_{A,0}$ and $\theta_B = \theta_{B,A}$ are the joint angles of the equivalent open-loop chain.

Note that $\theta_{9,0}$, $\theta_{7,0}$, and $\theta_{5,A}$ are the input actuator displacements. Combining Eqs. (12), (14), and (16), we obtain the structure matrix as:

$$\begin{aligned} A &= \begin{bmatrix} N_{8,9}N_{1,8} & N_{6,7}N_{1,6} & 0 \\ N_{8,9}N_{1,8}N_{2,1}N_{B,2} & 0 & -N_{4,5}N_{3,4}N_{B,3} \end{bmatrix} \\ &= \begin{bmatrix} 40.96 & 40.96 & 0 \\ 5.12 & 0 & -24 \end{bmatrix} \end{aligned} \tag{17}$$

It can be shown that the null vector for the above structure matrix is given by $[75, -75, 16]^T$. Hence, the sense of input actuator torques can be maintained either in the direction of $[+,-,+]^T$ or $[-,+,-]^T$.

DYNAMICAL EQUATIONS

The dynamical equations of motion can be derived by several methods (Craig, 1989, Paul, 1981, Thomas and Tesar, 1982). In what follows, we shall use a systematic approach recently developed by Chen et al (1990) for the analysis.

The kinetic energy of the system can be divided into two parts: (1) K_m contributed from the motion of major links A and B, assuming all the gears and shafts are rigidly attached to their corresponding carriers, and (2) K' contributed by the relative motion of the carried links. That is

$$K = K_m + K' \tag{18}$$

The first part of Eq. (18), K_m, can be written as

$$\begin{aligned} K_m &= \frac{1}{2}J'_A\dot{\theta}_A^2 + \frac{1}{2}m_A x_A^2\dot{\theta}_A^2 + \frac{1}{2}J'_B(\dot{\theta}_A + \dot{\theta}_B)^2 + \\ &\quad \frac{1}{2}m_B[l^2\dot{\theta}_A^2 + 2lx_B\dot{\theta}_A(\dot{\theta}_A + \dot{\theta}_B)\cos\theta_B + \\ &\quad x_B^2(\dot{\theta}_A + \dot{\theta}_B)^2] \end{aligned} \tag{19}$$

where l denotes the link length, θ the joint angle, m the combined mass of a major link and its carried links, x the distance

from the combined center of mass to its proximal joint axis, J the combined moment of inertia of an equivalent link about an axis passing through the center of mass and parallel to its proximal joint axis, and where the subscripts A and B refer to major links A and B, respectively.

Rearranging Eq. (19), yields

$$K_m = \frac{1}{2}J_A\dot{\theta}_A^2 + \frac{1}{2}J_B(\dot{\theta}_A + \dot{\theta}_B)^2 + \frac{1}{2}m_B(l^2\dot{\theta}_A^2 + 2lx_B\dot{\theta}_A^2\cos\theta_B + 2lx_B\dot{\theta}_A\dot{\theta}_B\cos\theta_B) \quad (20)$$

where J denotes the combined moment of inertia of an equivalent link about its proximal joint axis.

It has been shown that additional kinetic energy, $K'_{i,j}$, for a link i performing simple rotation with respect to an axis fixed to its carrier j is given by (Chen, 1989):

$$K'_{i,j} = \frac{1}{2}J_i(\dot{\theta}_{i,j})^2 + J_i\dot{\theta}_{i,j}(\underline{\omega}_j \cdot \underline{e}_i) \quad (21)$$

where J_i is the moment of inertia of a carried link i about its axis of rotation on link j, $\underline{e}_i$ is a positive unit vector defined along the axis of relative rotation, $\underline{\omega}_j$ is the angular velocity of link j with respect to the inertia frame.

For the prototype manipulator shown in Fig. 1, either the rotation axis of a carried link is perpendicular to the rotation axis of its carrier or the carrier itself is stationary (ground link). Hence, Eq. (21) reduces to

$$K'_{i,j} = \frac{1}{2}J_i\,(\dot{\theta}_{i,j})^2 \quad (22)$$

Substituting Eq. (8)-(16) into (22) and summing them, yields

$$\begin{aligned} K' = \frac{1}{2}[&J_1(\dot{\theta}_A + 0.125\dot{\theta}_B)^2 + J_2(0.5\,\dot{\theta}_B)^2 \\ &+J_3(-2\dot{\theta}_B)^2 + J_4(4.8\dot{\theta}_B)^2 \\ &+J_5(-24\dot{\theta}_B)^2 + J_6(-6.4\dot{\theta}_A)^2 \\ &+J_7(40.96\dot{\theta}_A)^2 + J_8(-6.4\dot{\theta}_A - 0.8\dot{\theta}_B)^2 \\ &+J_9(40.96\dot{\theta}_A + 5.12\dot{\theta}_B)^2] \end{aligned} \quad (23)$$

where J_i denotes the moment of inertia of a carried link i with respect to its rotation axis.

The Lagrange's equations of motion for the prototype arm can be written as:

$$\frac{d}{dt}\left(\frac{\partial K}{\partial\dot{\theta}_i}\right) - \frac{\partial K}{\partial\theta_i} = \tau_i, \qquad i = 1, 2. \quad (24)$$

where the θ's denote the generalized coordinates, and τ's the generalized active forces.

Substituting Eqs. (20) and (23) into (18) and then the resulting equation into (24), yields the dynamical equations as:

$$\tau_1 = (r + 2k\,\cos\theta_B)\ddot{\theta}_A + (s + k\,\cos\theta_B)\ddot{\theta}_B - 2k\,(\sin\theta_B)\,\dot{\theta}_A\dot{\theta}_B - k\,(\sin\theta_B)\,\dot{\theta}_B^2 \quad (25)$$

$$\tau_2 = (s + k\,\cos\theta_B)\ddot{\theta}_A + t\,\ddot{\theta}_B + k\,\sin\theta_B\,\dot{\theta}_A^2 \quad (26)$$

where

$$r = J_A + J_B + J_1 + 40.96J_6 + 40.96^2J_7 + 40.96J_8 + 40.96^2J_9 + m_Bl^2 \quad (27)$$

$$s = J_B + 0.125J_1 + 5.12J_8 + 5.12 \cdot 40.96J_9 \quad (28)$$

$$t = J_B + 0.125^2J_1 + 0.25J_2 + 4J_3 + 23.04J_4 + 576J_5 + 0.64J_8 + 5.12^2J_9 \quad (29)$$

$$k = m_Blx_B \quad (30)$$

Note that the dynamical equations contain only four independent parameters, r, s, t and k. If the J's and m's are known, then r, s, t and k can be calculated. If the J's and m's are not known, then r, s, t and k must be estimated experimentally. In general, J_A and J_B are a few order of magnitude greater than that of the rotors, gears, and shafts. However, the inertia effect of rotors can be as large as that of the major links, since they are multiplied by the square of the gear ratios as shown in the above equations.

COMPUTED TORQUE CONTROL LAW

The dynamical equations can be written in a matrix form as shown below:

$$\underline{G}\,\ddot{\underline{\theta}} + \underline{f}_r(\dot{\underline{\theta}}, \underline{\theta}) = \underline{\tau}\,. \quad (31)$$

where

$$\underline{G} = \begin{bmatrix} r + 2k\,\cos\theta_B & s + k\,\cos\theta_B \\ s + k\,\cos\theta_B & t \end{bmatrix} \quad (32)$$

is the mass matrix,

$$\underline{f}_r = -k\,\sin\theta_B \begin{bmatrix} 2\dot{\theta}_A\dot{\theta}_B + \dot{\theta}_B^2 \\ \dot{\theta}_A^2 \end{bmatrix} \quad (33)$$

is the matrix representing Coriolis and centrifugal forces, $\underline{\theta} = [\theta_A, \theta_B]^T$ are the generalized coordinates, and $\underline{\tau} = [\tau_1, \tau_2]^T$ are the generalized active forces.

Since joint angles, θ_A and θ_B, are used as the generalized coordinates, the generalized active forces are, in effect, the resultant joint torques about joint axes Z_1 and Z_2, respectively. In the design of a computed torque controller, Eq. (3) can be used to convert these joint torques into actuator torques.

I_1	44195	gm-cm^2	J_2	205	gm-cm^2
J_3	189	gm-cm^2	J_4	111	gm-cm^2
J_5	470	gm-cm^2	J_6	10102	gm-cm^2
J_7	1223	gm-cm^2	J_8	10102	gm-cm^2
J_9	1223	gm-cm^2	J_A	1195685	gm-cm^2
J_B	124005	gm-cm^2	m_A	5770	gm
m_B	515	gm	l	30.48	cm
x_B	11.04	cm			

Table 2: Inertia properties of the links.

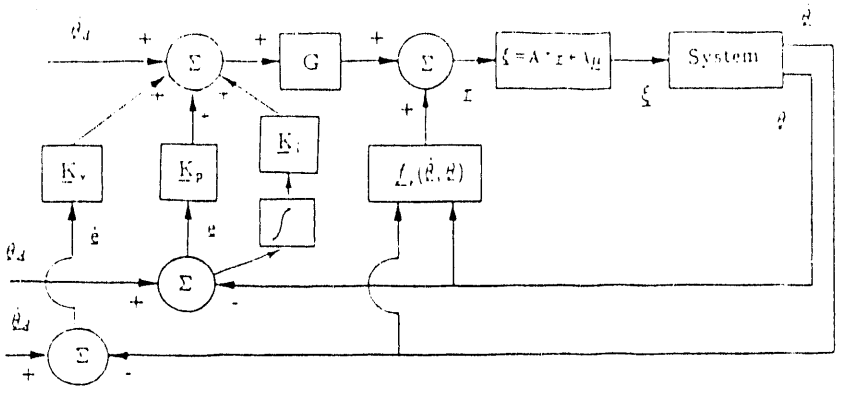

Figure 3: Computed Torque Control Flowchart

Using the computed torque technique, generalized active forces are computed in every sampling period by using the following equation:

$$\underline{\tau} = \underline{a}\ddot{\underline{\theta}}_d + \underline{a}\underline{k}_v\dot{\underline{e}} + \underline{a}\underline{k}_p\underline{e} + \underline{f}_r(\dot{\underline{\theta}}, \underline{\theta}) \tag{34}$$

where

$$\underline{e} = \underline{\theta}_d - \underline{\theta} \tag{35}$$

is the error signal, $\underline{\theta}_d$ is the desired joint angle, and $\underline{k}_p$ and $\underline{k}_v$ are the positional and velocity feedback gain matrices.

Substituting Eq. (34) into (31) and after simplification, yields

$$\ddot{\underline{e}} + \underline{k}_v\dot{\underline{e}} + \underline{k}_p = 0 \tag{36}$$

The position and velocity feedback gain matrices, $\underline{k}_p$ and $\underline{k}_v$, must be chosen properly such that the system is stable and the manipulator will follow a desired path. To correct steady-state error, the integration of position error is also added to the controller. The computed torque control flow chart for the RBR arm is shown in Fig. 3, where $\underline{k}_i$ is the integration feedback gain.

For the 2-DOF prototype arm, inertia properties of the rotors, gears, shafts, and the two major links are estimated from their sizes and materials used and are listed in Table 2. From the inertia properties given in Table 2, we obtain $r = 6773598$ gm-cm^2, $s = 437732$ gm-cm^2, $t = 437307$ gm-cm^2, and $k = 173297$ gm-cm^2.

In the experiment, the following values are chosen for $\underline{k}_p$ and $\underline{k}_v$ such that the system is critically damped.

$$\underline{k}_p = \begin{bmatrix} 0.84 & 0 \\ 0 & 0.84 \end{bmatrix} \tag{37}$$

and

$$\underline{k}_v = \begin{bmatrix} 1.833 & 0 \\ 0 & 1.833 \end{bmatrix} \tag{38}$$

MOTOR TORQUES AND POWER CONSUMPTION

Power Consumption with Redundant Drives

As discussed previously, the value of λ must be selected properly so that each actuator torque can be maintained in a predetermined direction. In the experimental arm, λ is determined by the principle of minimum power consumption.

The output torque of a DC motor is given by

$$\xi = k_\tau i \tag{39}$$

where k_τ is the torque constant and i the applied current. Hence, power loss due to motor impedance can be written as

$$p = i^2R = R\xi^2/k_\tau^2 = (\xi/Z)^2, \tag{40}$$

where R is the motor impedance and $Z = k_\tau/R^{0.5}$.

For the prototype two-DOF arm, the structure matrix is given by

$$A = \begin{bmatrix} g_1 & g_3 & 0 \\ g_2 & 0 & -g_4 \end{bmatrix}, \tag{41}$$

where $g_1 = g_3 = 40.96$, $g_2 = 5.12$, and $g_4 = 24.00$ are all positive numbers. Applying Eq. (3), we obtain motor torques in terms of joint torques as follows:

$$\begin{aligned} \underline{\xi} &= \frac{1}{\Delta}\begin{bmatrix} g_1g_4^2 & g_2g_3^2 \\ g_2^2g_3 + g_3g_4^2 & -g_1g_2g_3 \\ g_1g_2g_4 & -g_1^2g_4 - g_3^2g_4 \end{bmatrix}\underline{\tau} + \lambda\begin{bmatrix} g_3g_4 \\ -g_1g_4 \\ g_2g_3 \end{bmatrix} \\ &= \underline{X} + \lambda\underline{\mu} \end{aligned} \tag{42}$$

where $\underline{X}$ is the particular solution of $\underline{\xi}$ and,

$$\Delta = g_1^2g_4^2 + g_2^2g_3^2 + g_3^2g_4^2. \tag{43}$$

Note that the second component of the homogeneous solution, μ_2, is negative. Hence, the direction of torque applied by the second motor should be maintained in the negative sense at all times.

The power consumption of the system can be written as

$$P = \sum_{j=1}^{3}\left(\frac{\xi_j}{Z_j}\right)^2 \tag{44}$$

Substituting Eq. (42) into (44), yields

$$P = \sum_{j=1}^{3}\left(\frac{X_j + \lambda\,\mu_j}{Z_j}\right)^2 \tag{45}$$

Note that power consumption, P, is a parabolic function of λ. Its optimal value can be obtained by minimizing P subject to the following constraints

$$\begin{aligned} \xi_1 &= \lambda_1 + \lambda\mu_1 \geq 0, \\ \xi_2 &= \lambda_2 + \lambda\mu_2 \geq 0, \\ \xi_3 &= \lambda_3 + \lambda\mu_3 \geq 0. \end{aligned} \tag{46}$$

Substituting μ_i from Eq. (42) into Eq. (46), yields

$$\begin{aligned} \lambda &\geq -\frac{\lambda_1}{g_3 g_4} = \lambda_1 \\ \lambda &\geq -\frac{\lambda_2}{g_1 g_4} = \lambda_2 \\ \lambda &\geq -\frac{\lambda_3}{g_2 g_3} = \lambda_3. \end{aligned} \tag{47}$$

Let the minimum value of P occur at $\lambda = \lambda^*$. Then λ^* can be found by solving

$$\frac{\partial P}{\partial \lambda}\Big|_{\lambda=\lambda^*} = \sum_{i=1}^{3} 2\frac{\mu_i}{Z_i}\left(\frac{\lambda_i + \lambda\mu_i}{Z_i}\right) = 0, \tag{48}$$

which yields

$$\lambda^* = -\frac{\sum_{i=1}^{3}\left(\mu_i\lambda_i/Z_i^2\right)}{\sum_{i=1}^{3}\left(\mu_i/Z_i\right)^2} \tag{49}$$

It can be shown that $\mathrm{Min}(\lambda_1, \lambda_2, \lambda_3) \leq \lambda^* \leq \mathrm{Max}(\lambda_1, \lambda_2, \lambda_3)$. But $\lambda^* \geq \mathrm{Max}(\lambda_1, \lambda_2, \lambda_3)$ must also be satisfied. Hence, minimum power consumption occurs at $\lambda^* = \mathrm{Max}(\lambda_1, \lambda_2, \lambda_3)$. There are three operating regions:

1. Region I

$$\lambda^* = \lambda_1 = \mathrm{Max}(\lambda_1, \lambda_2, \lambda_3) \tag{50}$$

which implies

$$\begin{aligned} \tau_1 &\leq 0 \\ \tau_2 &\leq 0 \end{aligned} \tag{51}$$

Substituting Eqs. (42) and (50) into (45), yields

$$P = \left(\frac{\tau_1}{g_3 Z_2}\right)^2 + \left(\frac{\tau_2}{g_4 Z_3}\right)^2 = \left(\frac{\tau_1}{40.96 Z_2}\right)^2 + \left(\frac{\tau_2}{24 Z_3}\right)^2 \tag{52}$$

2. Region II

$$\lambda^* = \lambda_2 = \mathrm{Max}(\lambda_1, \lambda_2, \lambda_3) \tag{53}$$

which implies

$$\begin{aligned} \tau_1 &\geq 0 \\ g_2\tau_1 &\geq g_1\tau_2 \end{aligned} \tag{54}$$

Substituting Eqs. (42) and (53) into (45), yields

$$P = \left(\frac{\tau_1}{g_1 Z_1}\right)^2 + \left(\frac{g_2\tau_1 - g_1\tau_2}{g_1 g_4 Z_3}\right)^2 = \left(\frac{\tau_1}{40.96 Z_1}\right)^2 + \left(\frac{\tau_1 - 8\tau_2}{192 Z_3}\right)^2 \tag{55}$$

3. Region III

$$\lambda^* = \lambda_3 = \mathrm{Max}(\lambda_1, \lambda_2, \lambda_3) \tag{56}$$

which implies

$$\begin{aligned} \tau_2 &\leq 0 \\ g_2\tau_1 &\leq g_1\tau_2 \end{aligned} \tag{57}$$

Substituting Eqs. (42) and (56) into (45), yields

$$P = \left(\frac{\tau_2}{g_2 Z_1}\right)^2 + \left(\frac{g_2\tau_1 - g_1\tau_2}{g_2 g_4 Z_2}\right)^2 = \left(\frac{\tau_2}{5.12 Z_1}\right)^2 + \left(\frac{\tau_1 - 8\tau_2}{40.96 Z_2}\right)^2 \tag{58}$$

Power Consumption without Redundant Drives

Although the prototype arm is designed with redundant drives, it can also function as a conventional robot arm. This is accomplished by disconnecting motor 1 from the first transmission line. It is obvious that power consumption for such a conventional two-DOF manipulator is given by

$$P = \left(\frac{\tau_1}{g_3 Z_2}\right)^2 + \left(\frac{\tau_2}{g_4 Z_3}\right)^2 = \left(\frac{\tau_1}{40.96 Z_2}\right)^2 + \left(\frac{\tau_2}{24 Z_3}\right)^2 \tag{59}$$

Note that power consumption due to motor impedance depends on the gear ratios. Also note that when the RBR arm is operating in "Region I," its power consumption is identical with that of a conventional manipulator. However, when the RBR arm is operating in "Regions II and III," its power consumption can be much higher than that of a conventional manipulator. The motor constants for the experimental arm are $Z_1 = Z_2 = 83.26 mNm/\sqrt{\mathrm{W}}$ and $Z_3 = 55.6 mNm/\sqrt{\mathrm{W}}$.

EXPERIMENTAL VERIFICATION

To establish a proof of the concept, two experiments were conducted, one with and the other without backlash control.

In the first experiment, conventional control was used. Although the prototype arm was designed with unidirectional redundant drives, it can also function as a conventional robot arm with no positive control on backlash. This is accomplished by disconnecting one of the three drive lines. Since motors 2 and 3 drive joints 1 and 2 independent of each other, these two motors were selected as the drivers for the experiment while the third motor was physically disconnected. In this case, actuator torques were related to the resultant joint torques by: $[\xi_2, \xi_3]^T = [\tau_1/40.96, -\tau_2/24]^T$.

In the second experiment, backlash was controlled by redundant drives. Using computed torque control technique, all three motors were driven simultaneously to manipulate the robot arm. The value of λ was computed by using the principle of minimal power consumption described in the previous section, and actuator torques were computed by using the pseudo inverse transformation. We note that the pseudo inverse and the null vector of the structure matrix A are constant terms and need not be computed on line. A simple PID controller was designed. An IBM Model 55, 80386SX, Personal Computer was used for all the necessary computations and control commands. A Hewlett-Packard Bipolar Power Supply/Amplifier was used to supply required currents to the motors.

A laser tracking system developed by NIST (National Institute of Standard and Technology) was used to measure the Cartesian coordinates of a reference point at the end of link B. The experiments were performed at four different postures (i.e.

end-effector position and the manipulator to ensure a good coverage of the work space. For each posture, a target point was selected by bringing the end-effector to a predetermined position. Then the robot arm was commanded to approach the target point from four orthogonal directions in the joint space, i.e. from four different combinations of plus and minus directions of rotation about the two joint axes. This yielded maximal backlash effects on repeatability. For each direction of approach, fifteen measurements were made to ensure statistically meaningful results.

Repeatability is a measure of the ability of a manipulator to repeatedly bring its end effector back to a previously taught position. Since the prototype is a planar manipulator, all data points should theoretically fall on one plane. In practice, however, a small deviation from the plane may occur due to mechanical clearances in the joints and due to flexibility of the links. In this paper, we define the radius of the smallest ball containing the sixty data points taken from four directions of approach as the *repeatability* of the manipulator. We note that bringing the manipulator to a taught point from four orthogonal directions in the joint space does not necessarily result in four orthogonal paths in the task space.

Appendix A shows some typical repeatability data taken for one posture of the manipulator. Because of space limitation, we have included only the data for the first and second directions of approach in the Appendix. More detailed repeatability data can be found in Chang's dissertation (1991).

We note that when the manipulator was repeatedly brought back to a target point from the same direction of approach, the end-effector had a tendency to settle on the vicinity of a point, which may or may not necessarily be the target point, to within a fraction of a millimeter .

The experimental data indicates that the end-effector was always capable of coming back to the target point to within a fraction of a millimeter when it was controlled by three redundant motors. However, when the manipulator was controlled without redundant drives, the repeated positions were not necessarily be the target point. Specifically, under conventional control, the repeated position was often close to the target point when it was brought back from the first direction of approach, while it was always a few millimeters away from the target point when it was brought back from the second, third, or the fourth direction. This is due to the fact that the target point was chosen by servoing the manipulator into the position from the first direction of approach. When external disturbances and noises were small, free play tended to fall on the same side of gear meshes and, consequently, the end-effector was capable of coming back to the vicinity of a position repeatedly. However, when external disturbances were large, free play could occur randomly which resulted in poor repeatability even when the manipulator was commanded to approach the target point from the first direction. Commanding the manipulator to approach the target point from four different directions ensures that backlash will occur on both sides of gear meshes and, therefore results maximal effect on repeatability.

Table 3 shows the differences in repeatability calculated from the measurements made at NIST. We conclude that the repeatability of the prototype arm with redundant drives is one order-of-magnitude smaller than that without redundant drives. Specifically, the average repeatability is 0.4004 mm with redundant drives as compared to 4.6971 mm without redundant drives.

Manipulator Posture	Repeatability (mm)	
	Conventional Control	Redundant Control
1	6.388480	0.3985681
2	6.611162	0.1786238
3	3.195182	0.1188081
4	2.593668	0.3054367

Table 3: Comparison of Repeatability

SUMMARY

The concept of RBR mechanisms is demonstrated with a prototype manipulator. In general, it is shown that gear backlash in an n-DOF manipulator can be eliminated by using a minimum of $(n+1)$ unidirectional drives. In this study, we have designed and constructed a two-DOF manipulator with three unidirectional drives. Then dynamical equations of motion for the manipulator, including inertia effect of gears and rotors, are derived. It is shown that inertia effect of the rotors can be as large as that of the major links and they should not be neglected in the dynamic model. A PID controller using computed torque technique has been designed and implemented. A method for computing redundant motor torques with minimal power consumption has been developed. And finally, two experiments were conducted to verify the concept. The experimental results demonstrate that the repeatability of a manipulator with redundant drives is one order-of-magnitude better than that without redundant drives. This concept is equally applicable to other geared servomechanisms including NC machines.

ACKNOWLEDGMENT

This work was supported in part by the U.S. Department of Energy under Grant DEF05-88ER13977, and in part by the NSF Engineering Research Centers Program NSFD CDR 8803012.

REFERENCES

1. Broderick, P.L., and Cipra, R.J., 1988, "A Method for Determining and Correcting Robot Position and Orientation Errors Due to Manufacturing," *ASME Trans., J. of Mechanisms, Transmissions, and Automation in Design*, Vol. 110, No. 1, pp. 3-10.

2. Calson, J. H., 1985, "Harmonic Drives for Servomechanisms," *Machine Design*, Vol. 57, No. 1, pp. 102-106.

3. Chang, S.L., 1991, "Redundant-drive Backlash-free Robotic Mechanisms: Mechanisms Creation, Analysis, and Control," Ph.D. dissertation, Mechanical Engineering Department, The University of Maryland, College Park, MD 20742.

4. Chang, S. L., and Tsai, L. W., 1990a, "Topological Synthesis of Articulated Gear Mechanisms," *IEEE Trans. on Robotics and Automation*, Vol. 6, No.1 pp.97-103.

5. Chang, S. L., and Tsai, L. W., 1990b, "On the Redundant-

Drive Backlash Free Robotic Mechanisms," accepted for publication in *ASME Trans., J. of Mechanical Design*, also in ASME publication, Cams, Gears, Robot and Mechanism Design, DE Vol. 26, pp. 255-262, Sept. 1990.

6. Chao, L.M., and Yang, J.C.S., 1986, "Development and Implementation of a Kinematic Parameter Identification Technique to Improve the Positioning Accuracy of Robots," *Proc. of SME Conf., Robots 10*, MS86-424, Chicago, Ill.

7. Chen, J., 1989, "The Effect of Gear Reduction on Robot Dynamics," *NASA Telerobotic Conference*, Pasadena, Calif.

8. Chen, J., Chen, D.Z., and Tsai, L.W., 1990, "A Systematic Methodology for the Dynamic Analysis of Articulated Gear-Mechanisms," *Proc. of Japan-U.S.A. Symposium on Flexible Automation*, Kyoto, Japan, Vol. 1, pp. 273-278.

9. Dagalakis, N. G., and Myers, D. R., 1985, "Adjustment of Robot Joint Gear Backlash using Robot Joint Test Excitation Technique," *The International J. of Robotics Research*, Vol. 4, No. 2.

10. Klein, C. A., and Huang, C. H., 1983, "Review of Pseudo-Inverse Control for Use with Kinematically Redundant Manipulators," *IEEE Trans. on System, Man, and Cybernetics*, Vol. SM513, pp. 245-250.

11. Michalec, G. W., 1966, Precision Gearing: Theory and Practice, John Wiley & Sons, Inc., New York

12. Paul, R.P., 1981, "Robot Manipulators: Mathematics, Programming, and Control," MIT Press, Cambridge, Mass.

13. Thomas, M., and Tesar, D., 1982, "Dynamic Modeling of Serial Manipulator Arms," *ASME Trans., J. of Mechanisms, Transmissions, and Automation in Design*, Vol. 104, pp. 218-228.

14. Sweet, L.M., 1991, "People and Technology in Globally Competitive Factory," *IEEE Control Systems*, Vol. 11, No. 7, pp. 4-8.

15. Tsai, L.W., 1988, "The Kinematics of Spatial Robotic Bevel-Gear Trains," *IEEE J. of Robotics and Automation*, Vol. 4, No. 2, pp. 150-156.

16. Veitschegger, W. K., and Wu, C. H., 1986, "Robot Accuracy Analysis Based on Kinematics," *IEEE J. of Robotics and Automation*, Vol. 2, No. 3, pp. 171-179.

APPENDIX A: EXPERIMENTAL DATA

Conventional Control

Target point:

x = 486.980653, y = 1593.003201, z = -24.167939 (mm)

x (mm)	y (mm)	z (mm)
First Direction of Approach:		
486.738812	1592.854887	-24.181058
485.838051	1592.397990	-24.195490
486.044833	1592.500472	-24.185105
485.146270	1592.036758	-24.195382
487.198320	1593.045755	-24.184805
487.295308	1593.047007	-24.197293
487.199899	1592.979187	-24.189253
487.223137	1592.994359	-24.182124
487.348397	1593.075724	-24.178663
487.471829	1593.079152	-24.168273
487.524474	1593.082279	-24.165431
487.443514	1593.059934	-24.162886
487.388828	1593.022979	-24.167933
487.295605	1592.949973	-24.174437
487.121221	1592.949643	-24.178204
Second Direction of Approach:		
482.394973	1590.692488	-24.231879
481.365708	1590.565643	-24.213858
483.728381	1591.302381	-24.212662
482.598364	1590.732747	-24.214337
482.020435	1590.644426	-24.214918
483.086993	1590.989286	-24.209940
482.074189	1590.590342	-24.210482
481.796526	1590.605994	-24.212614
481.716057	1590.540913	-24.213590
482.272578	1590.647182	-24.204713
483.690968	1591.277406	-24.199527
483.695307	1591.281220	-24.199106
481.360564	1590.538643	-24.221945
482.119978	1590.586930	-24.218017
482.250586	1590.663333	-24.211607

Backlash Control using Redundant Drives

Target point:

x = 309.167663, y = 1857.337207, z = 18.949129 (mm)

x (mm)	y (mm)	z (mm)
First Direction of Approach:		
308.939150	1857.237822	-18.956039
308.854455	1857.220513	-18.972659
308.894433	1857.223181	-18.955600
309.366945	1857.374911	-18.949773
308.885230	1857.221213	-18.941603
309.321275	1857.394571	-18.947685
309.329459	1857.405601	-18.943533
309.204785	1857.354006	-18.945216
309.376551	1857.426493	-18.941085
308.926891	1857.259355	-18.952369
309.161527	1857.364255	-18.945169
308.888587	1857.202343	-18.971058
308.883715	1857.237595	-18.959370
308.959667	1857.261740	-18.954539
309.200073	1857.354639	-18.944316
Second Direction of Approach:		
309.370723	1857.420249	-18.940705
309.412143	1857.429364	-18.943211
309.354632	1857.392413	-18.944870
309.422384	1857.419854	-18.922082
309.326861	1857.366102	-18.942879
309.164434	1857.349884	-18.938623
309.213349	1857.331150	-18.954877
309.309834	1857.367852	-18.939250
309.376247	1857.370224	-18.958897
309.343227	1857.410008	-18.947078
309.432581	1857.401629	-18.938312
309.293248	1857.384313	-18.948524
309.286263	1857.391899	-18.947806
309.311359	1857.381330	-18.929589
309.432830	1857.454309	-18.943020

END

DATE
FILMED
8/13/92